IEEE Photonics Journal
An IEEE Photonics Society Publication

Open Access

Single-Polarization Waveguiding by Low-Index Strips on the Surface of Chalcogenide Glass Film

Volume 8, Number 2, April 2016

Yanfen Zhai
Renduo Qi
Chenzhi Yuan
Shuai Dong
Wei Zhang
Yidong Huang

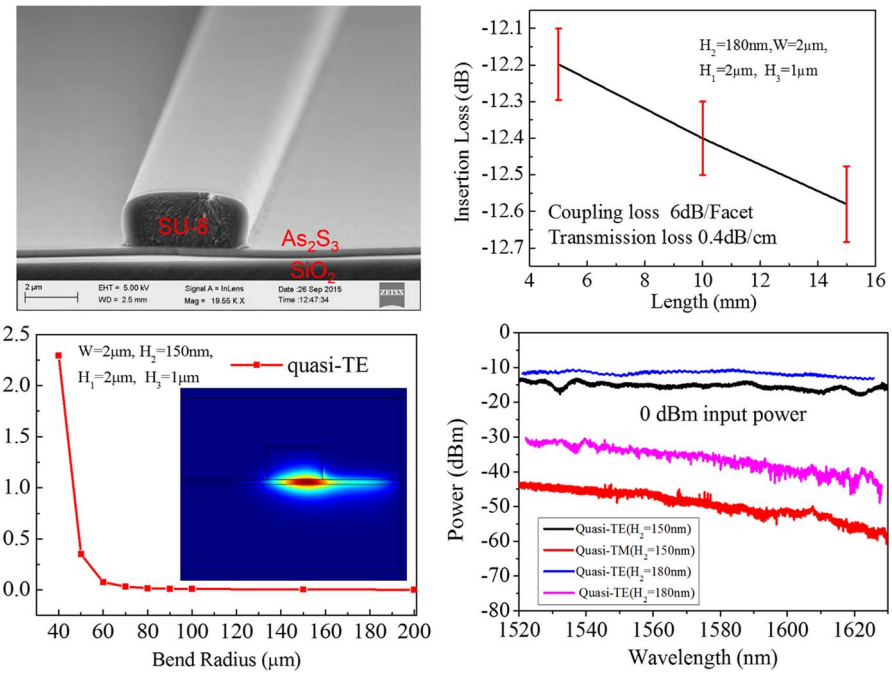

DOI: 10.1109/JPHOT.2016.2531598
1943-0655

Single-Polarization Waveguiding by Low-Index Strips on the Surface of Chalcogenide Glass Film

Yanfen Zhai, Renduo Qi, Chenzhi Yuan, Shuai Dong, Wei Zhang, and Yidong Huang

Tsinghua National Laboratory for Information Science and Technology, Department of Electronic Engineering, Tsinghua University, Beijing 100084, China

DOI: 10.1109/JPHOT.2016.2531598

Manuscript received February 1, 2016; accepted February 13, 2016. Date of publication February 18, 2016; date of current version March 1, 2016. This work was supported by the 973 Programs of China under Contract 2013CB328700 and Contract 2011CBA00303, by the National Natural Science Foundation of China under Contract 61575102 and Contract 61321004, by the Tsinghua University Initiative Scientific Research Program under Contract 20131089382, and by the Basic Research Foundation of Tsinghua National Laboratory for Information Science and Technology (TNList). Corresponding author: W. Zhang (e-mail: zwei@tsinghua.edu.cn).

Abstract: In this paper, we propose and demonstrate a simple chalcogenide glass (ChG) waveguide structure, which is composed of a low refractive-index strip on the surface of the planar ChG film. Theoretical analysis shows that it supports single quasi-TE mode transmission at 1.55 μm with high third-order nonlinearity and negligible bending loss if the bending radius is higher than 60 μm. Then, the ChG waveguide is fabricated and measured. For the waveguide sample with a ChG film of 180 nm in thickness, the measured attenuation of the quasi-TE mode is 0.4 dB/cm at 1.55 μm. Meanwhile, the extinction ratio between the two polarization modes in the waveguide sample of 10 mm in length is higher than 25 dB over a region of 80 nm at 1.55 μm. For the waveguide sample with similar length and a smaller ChG film thickness (150 nm), the extinction ratio increases to 35 dB. These results demonstrate its property of low-loss single-polarization transmission. It provides a simple way to realize high-quality ChG waveguides, which have great potential on integrated nonlinear optical devices.

Index Terms: Chalcogenide glass (ChG), ChG film, ChG waveguide, single polarization transmission.

1. Introduction

Chalcogenide glass (ChG) has high third-order nonlinearity [1], [2], low two-photon absorption [2], and negligible free carrier absorption [2], [3], which are suitable for integrated photonic devices for nonlinear optics. Waveguides are basic units for integrated photonic devices. To fabricate ChG waveguides, the ChG films are usually first deposited on low index substrates, which can be realized by thermal evaporation [4], sputtering [5], chemical vapor deposition [6], and pulsed laser deposition [7]. To reduce the scattering loss, the annealing process should be applied on the ChG films [8]–[11] to relax the chemical bonds in the glass [12], [13]. Then, waveguide structures could be fabricated in the ChG films by several ways [14]. The most popular methods include wet etching [15], dry etching [16] and lift-off [17]. These processes always lead to the roughness on the side walls of the waveguides, which is the main reason for the

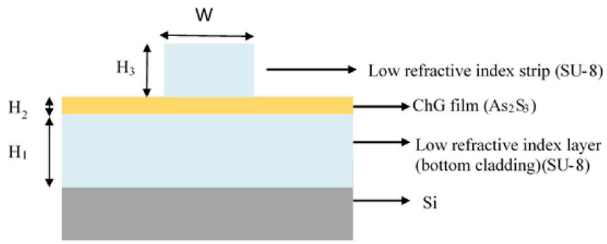

Fig. 1. Cross-section of the proposed waveguide.

attenuation of the ChG waveguides. Furthermore, the commercial (NH4OH)-based developers for UV-lithography or E-beam lithography may lead to pinhole formation and film peeling on the ChG film [12], [13], which may also reduce the quality of the ChG waveguides. Although the techniques of protective coating are developed to protect the ChG films, they make the waveguide fabrication process more complicated, and may also introduce additional loss on the ChG waveguides [12], [13], [18]–[23]. Recently, the fabrication processes of ChG films based on their organic ammonia solution attract much attention [24]. However, the residual solvent may lead to the obvious loss when it is used to fabricate optical waveguides in the near-infrared band, since its N-H bonds have an overtone absorption around 1510 nm [24]. On the other hand, ChG films fabricated by this way usually have pores, which may farther reduce the performances of ChG waveguides based on these films [25].

In this paper, we proposed and demonstrated a simple ChG waveguide structure, in which the light is guided by a low refractive-index strip on the surface of a planar ChG film. Since the light is mainly guided in the high index ChG film without any side wall, high transmission performance could be expected. Theoretical analysis shows that it supports single quasi-TE mode transmission at 1.5 μm with high third-order nonlinearity and low bending loss. Then, we fabricated the ChG waveguide sample and demonstrated its low loss single polarization transmission property experimentally. Since the lift-off process and various etching processes on the ChG films are avoided, the fabrication of the ChG waveguide is highly simplified. It provides a promising way to realize high quality ChG waveguides, which have great potential in integrated nonlinear optical devices.

2. Theoretical Analysis of the Proposed Waveguide Structure

Fig. 1 shows the proposed waveguide structure. On the silicon substrate, there is a thick layer of low refractive index dielectric materials as the bottom waveguide cladding. On the low index layer, a planar ChG thin film is deposited. Then, a strip of the low index dielectric material is fabricated on the ChG thin film as the guiding layer. In this waveguide structure, the light field is confined within the ChG film by the high index difference between the ChG film and the low index dielectric material in the vertical direction. Meanwhile, in the horizontal direction, the light field is guided along the low index strip on the top.

The transmission properties of the waveguide are analyzed theoretically by a software based on the finite element method (COMSOL Multiphysics). In order to calculate the leaky loss of the transmission modes, the boundary condition of the perfectly matched layer (PML) is used around the area of the waveguide structure [26]. The wave impedance of PMLs matches that of the adjacent medium in the waveguide area. Hence, the wave arrives the surface of PMLs would enter the PML regions without reflection. On the other hand, the index of the PML region has large imaginary part, hence the wave attenuate rapidly in the PML region, realizing the function of absorbing boundary.

First, the mode field profiles and the complex effective indices of the transmission modes are calculated. The structure parameters used in the calculation are selected according to the waveguide sample we fabricated and measured in the experiments, which are shown in Table 1. The material of the ChG film is As_2S_3, with a refractive index of 2.437@1550 nm [27]. The low index

TABLE 1

Structure Parameters of the Fabricated Waveguide Sample

Thickness of the SU-8 layer (H_1)	Thickness of the As_2S_3 layer (H_2)	Width of the SU-8 strip (W)	Height of the SU-8 strip (H_3)
2μm	180 or 150 nm	2μm	1μm

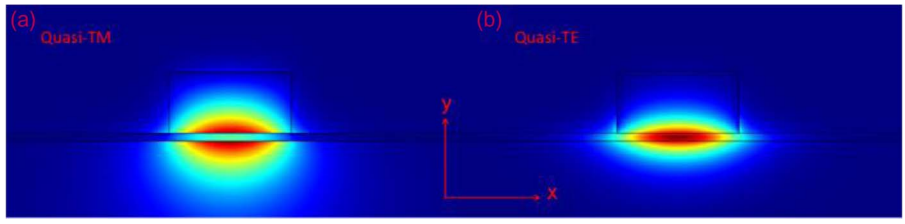

Fig. 2. Field distributions of (a) the fundamental quasi-TM mode and (b) the fundamental quasi-TE mode.

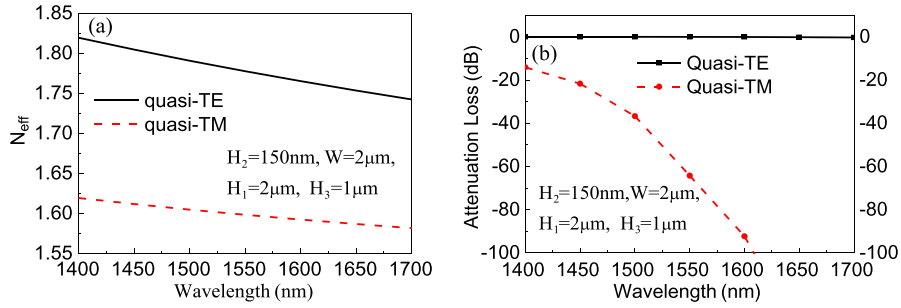

Fig. 3. Calculated effective indices (N_{eff}) of the quasi-TE mode and quasi-TM mode in the proposed waveguide. (a) Real parts of N_{eff} under different wavelength. (b) Attenuations of the two modes under different wavelengths, which are calculated by the imaginary parts of N_{eff} according to (1).

material for the bottom cladding and the strip is SU-8, which is a chemically amplified epoxy-based negative photoresist and has a refractive index of 1.56@1550 nm [28].

Fig. 2(a) and (b) show the calculated electric field distribution of the fundamental quasi-TM mode and the fundamental quasi-TE mode at 1550 nm, respectively. It can been seen that the mode fields of both modes are confined by the low index strip in horizon direction. In the vertical direction, the mode field of the quasi-TE mode is concentrated in the As_2S_3 layer, while the mode field of the quasi-TM mode is mainly distributed in the region of the low index strip and the bottom cladding.

The effective index (N_{eff}) of the fundamental quasi-TE and quasi-TM modes in this waveguide are calculated and shown in Fig. 3. Fig. 3(a) shows the real part of N_{eff} under different wavelengths. It can be seen that the real part of N_{eff} decreases with increasing wavelength for both modes. The real part of N_{eff} of the quasi-TM mode is much smaller than that of the quasi-TE mode, since its mode field mainly distributes in the low index region. As the wavelength increases, the real part of N_{eff} of the quasi-TM mode is gradually close to the index of SU-8, indicating that it is close to the cutoff condition of the mode and its leaky loss would increase with the increasing wavelength.

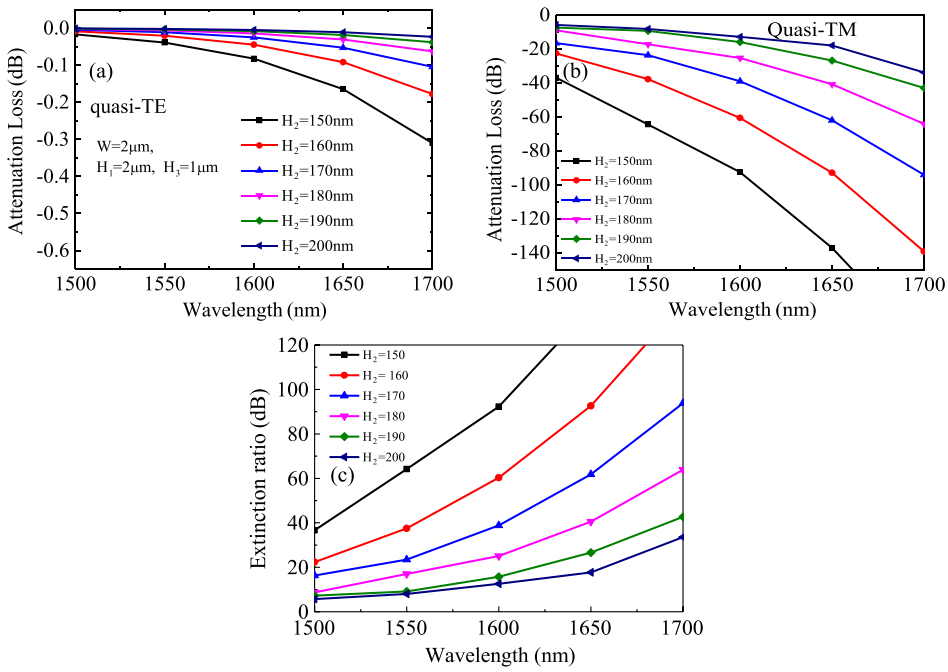

Fig. 4. Losses of the quasi-TE and quasi-TM modes in waveguides with different ChG layer thicknesses (H_2). The waveguide length is set at 10 mm. The loss spectra of (a) the quasi-TE mode and (b) the quasi-TM mode. (c) Extinction ratio of the two modes.

The attenuation of the two modes can be calculated by the imaginary part of the effective index N_{eff}

$$L_p = 8.687 \times \text{Im}(N_{\text{eff}}) k_0 l_0 \quad (\text{in dB}) \tag{1}$$

where k_0 is the wave number in vacuum ($k_0 = 2\pi/\lambda_0$), and l_0 is the waveguide length. It can be seen in Fig. 3(b) that the attenuation of the quasi-TE mode is quite low at all the wavelengths, showing that it is a guided mode in the whole wavelength range of the calculation. On the other hand, the attenuation of the quasi-TM mode increases with increasing wavelength. It is higher than 35 dB/cm, showing that the quasi-TM mode in this waveguide is cutoff at telecom band. Hence, this waveguide show the property of single polarization transmission over a broad band at telecom band.

It can be expected that the light confinement in vertical direction highly depend on the thickness of the ChG layer, which would impact the cut-off condition of the two modes. To show it more clearly, we calculated the losses of the two modes in the waveguides with different ChG layer thickness. The length of the waveguide is set at 10 mm. The calculation results are shown in Fig. 4. Fig. 4(a) is the result of the loss spectra of the quasi-TE mode with different ChG layer thickness. It can be seen that, for all the ChG layer thickness, the loss of the quasi-TE mode is very low at short wavelength region. On the other hand, the loss rises with increasing wavelength at long wavelength region, showing that the mode is close to the cutoff condition. Hence, the quasi-TE mode supports low loss transmission at telecom band (1.55 μm). It also shows that the loss rises at short wavelength if the waveguide has a thinner ChG layer, since the light confinement in the vertical direction is weaker. Since the quasi-TE mode can still be the transmission mode while the quasi-TM mode is cutoff at the same wavelength, the loss of quasi-TM mode is far higher than that of quasi-TE mode. Hence, the waveguide would act as an on-chip polarizer. Fig. 4(b) shows the attenuation loss of the quasi-TM mode. Fig. 4(c) shows the extinction ratio between the losses of quasi-TE mode and quasi-TM mode under different ChG film thickness. It can be seen that the extinction ratio rises with increasing wavelength for all of the

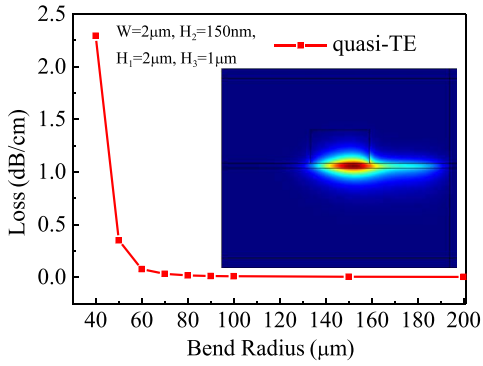

Fig. 5. Bending loss of the fundamental quasi-TE mode under different bending radii. The inset is the calculated modal field distribution under a bending radius of 50 μm.

ChG layer thickness. Thinner ChG layer leads to higher extinction ratio, since the loss of the quasi-TM mode increases more rapidly than that of the quasi-TE mode as the ChG layer thickness decreases. It can been seen that when the thickness of the ChG layer changes from 200 nm to 150 nm, the waveguide with a length of 10 mm can realize an on-chip polarizer with an extinction ratio ranging from 10 dB to 80 dB at the wavelength of 1550 nm.

By the commercial FEM software, the leaky loss due to the waveguide bending also can be calculated using a 2-D axisymmetric model, in which the cross section of the waveguide structure is plotted in the equal ϕ plane of the cylindrical coordinates. Fig. 5 is the calculated results of the fundamental quasi-TE mode under different bending radiuses. The inset of the figure is the modal field distribution under a bending radius of 50 μm. The waveguide bending leads that the modal field shifts to outer side of the waveguide. The main part is still in the waveguide region; however, it will lead to additional bending loss. The results in Fig. 5 shows that the bending loss would increase rapidly if the bending radius is smaller than 60 μm. When bending radius is 100 μm, the bending loss is about 0.008 dB/cm. Hence, the bending loss of this waveguide structure is negligible under a bending radius of hundreds μm. This property is better than that of the weak guiding waveguides used in traditional silica plane light circuits, which usually requires a bending radius of several millimeters due to its small index difference between its core and cladding.

To demonstrate its potential on nonlinear photonic devices, the effective area (A_{eff}) and the third order nonlinear coefficient (γ) of the quasi-TE mode under different wavelengths are also calculated by [29]–[31]

$$A_{\text{eff}} = \frac{\left|\int (\mathbf{e} \times \mathbf{h}^*) \cdot \hat{z} dA\right|^2}{\left|\int (\mathbf{e} \times \mathbf{h}^*) \cdot \hat{z}\right|^2 dA} \tag{2}$$

$$\gamma = \left(\frac{2\pi}{\lambda}\right) \frac{\int n_2 [(\mathbf{e} \times \mathbf{h}^*) \cdot \hat{z}]^2 dA}{\left[\int (\mathbf{e} \times \mathbf{h}^*) \cdot \hat{z} dA\right]^2} \tag{3}$$

where **e** and **h** are the electric field and magnetic field distributions of the mode, respectively. n_2 is the nonlinear Kerr index of the ChG material. Fig. 6 shows the calculation results at different wavelength. It can be seen that the A_{eff} increases with increasing wavelength. The effective mode area is about 1.18 μm^2 at 1550 nm with the structure parameters used in the calculation. However, the nonlinear coefficient decreases with increasing wavelength. It is about 9.9 /W/m at 1550 nm, which is about four orders of magnitude larger than that of silica fibers and one order of magnitude smaller than typical silicon wire waveguides [32]. Comparing with silicon wire waveguides, ChG waveguides have low two photon absorption and no free carrier absorption, leading to a good nonlinear figure of merit (FOM), which is 420 times higher than that of silicon

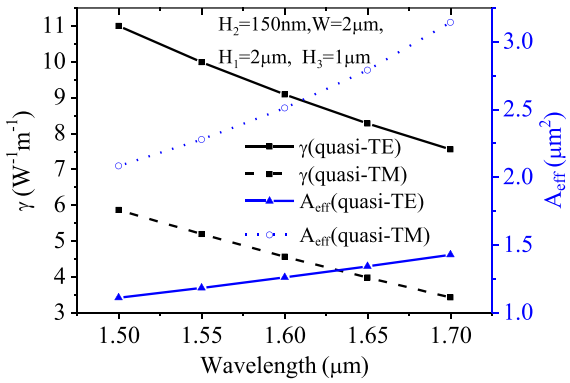

Fig. 6. Effective areas and the third order nonlinearity coefficients of the fundamental quasi-TE and quasi-TM modes under different wavelengths.

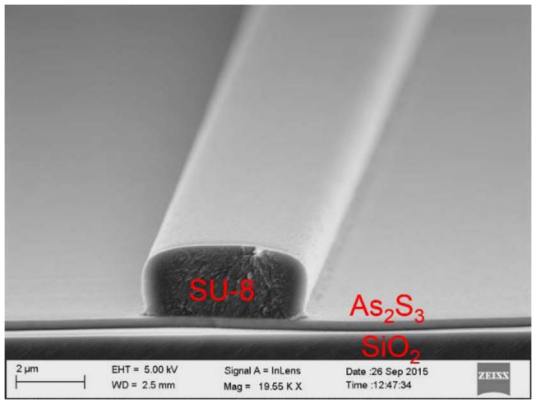

Fig. 7. SEM image of the cross section of the fabricated waveguide.

wire waveguide [11], [15]. Hence, comparing with silicon waveguides, the relatively low nonlinear coefficient can be compensated by longer waveguide length and higher pump light power.

3. Waveguide Fabrication and Measurement

The proposed waveguide structure was fabricated to demonstrate its transmission property. Firstly, a thick SU-8 layer was spin-coated on a silicon substrate and then cured by UV exposure. Then, an As_2S_3 film with a thickness of 150 nm/180 nm was deposited on the SU-8 layer by the thermal evaporation. After the evaporation, the sample was annealed in vacuum at 130 °C for 24 hours. Finally, the SU-8 strip was fabricated on the As_2S_3 film by UV lithography. This process avoids the lift-off process and the etching process on the As_2S_3 film. Fig. 7 shows the scanning electron microscopic (SEM) picture of the cross section of the waveguide. The structure parameters of the waveguide sample are shown in Table 1.

The transmission property of the waveguide is measured by an automatic alignment system (Apico-562) with a tunable laser (Santec TSL-510), which has a broad bandwidth from 1520 nm to 1630 nm. The light is coupled into and out of the waveguide by lensed fibers mounted on the alignment system. A polarization controller (Agilent, 11896 A) is used to control the light polarization to stimulate the quasi-TE or quasi-TM mode of the waveguide. The output light is detected by a power meter (Agilent 8164B).

We measured the insertion losses of the quasi-TE mode at 1550 nm in several waveguide samples with different lengths (5 mm, 10 mm, and 15 mm, respectively) and show the results in Fig. 8. By the linear fitting on the experimental results, the attenuation of the quasi-TE mode in

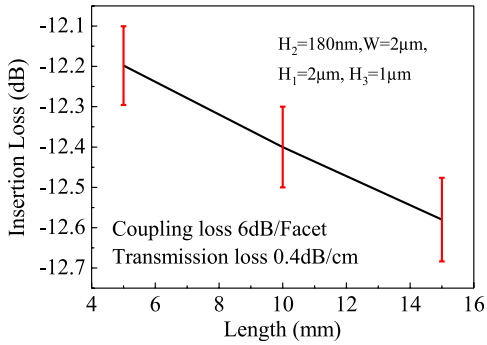

Fig. 8. Insertion losses of the quasi-TE mode in the waveguides with different lengths (5 mm, 10 mm, and 15 mm, respectively).

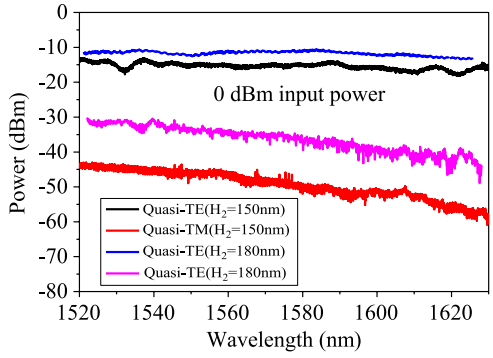

Fig. 9. Measured transmission spectrum of a waveguide sample with a length of 10 mm.

the waveguides can be estimated by the slope of the fitting line, which is about 0.4 dB/cm at 1550 nm. Meanwhile, the coupling loss between the waveguide and the lensed fibers can be estimated by the interception of the fitting line, which is 6 dB/facet. The experimental results demonstrate that the fabricated waveguides support low loss transmission in the telecom band by the quasi-TE mode. It is worth noting that the performance of the waveguide samples does not reduce for several months, showing that the oxidation of the ChG film is not a serious problem for these waveguides. Considering its potential application on integrated photonic devices, this problem can be solved completely by packaging the sample in a holder with inactive gases, such as nitrogen.

Fig. 9. shows the transmission spectrum of the quasi-TE mode, showing that the quasi-TE mode is a guided mode in the whole wavelength range we measured (1520 nm to 1630 nm). On the other hand, quasi-TM mode shows a clear cutoff property. When the thickness of CHG is 180 nm, the extinction ratio is 25 dB (at 1550 nm); when the thickness reduces to 150 nm, the extinction ratio is 35 dB (at 1550 nm). The insertion loss of the quasi-TE mode is about 12 dB mainly due to the coupling loss between the waveguide and fibers since no taper structures are designed at the ends of the waveguide.

For on-chip applications, a low loss polarizer with an ultra-small attenuation loss and high extinction ratio is desired [33]. Many TE-pass or TM-pass polarizers have been proposed theoretically or demonstrated experimentally. However, we notice that most of them only show theoretical analysis [34]–[38]. In order to achieve high extinction ratio, metal clad waveguides [36], [37], shallowly etched waveguides [26], gap plasmon waveguides are often adopted [39], [40]. These fabrication processes are complicated [39]–[42] or have significant insertion loss for the transmission mode [37]. However, to the best of our knowledge, there is no report on chalcogenide-based polarization manipulation devices. We also notice that as the CHG waveguide preparation

technology is increasingly more mature, some deposition techniques with fine thickness control have been developed. For example, in [43], the deposition rate of CHG films was stabilized at 20 Å s^{-1}. According to the theoretical calculation, the single polarization properties of the waveguide is mainly decided by the CHG film thickness; therefore, it can be expected that a polarizer with higher extinction ratio can be achieved by reducing the thickness of the CHG film.

4. Summary

In this paper, we proposed and demonstrated a simple ChG waveguide structure, which has a planar ChG film with a low refractive-index strip on its surface. In vertical direction the light field is confined in the ChG film, while in the horizon direction the light field is guided by the low index strip on the ChG film. Since the lift-off process and various etching processes on the ChG films are avoided, its fabrication is highly simplified. Theoretical analysis shows that it supports single quasi-TE mode transmission at 1.55 μm with high third-order nonlinearity and low bending loss if the bending radius is higher than 60 μm. Then, the ChG waveguide sample is fabricated and measured. In the fabrication process, the ChG films are realized by the As_2S_3 material using the thermal evaporation, and the low refractive index bottom cladding layer and strip on the surface are realized by SU-8 using UV lithography. Its transmission properties are measured by a tunable laser using the cut-off method. For a waveguide sample with a length of 10 mm and a ChG film thickness of 180 nm, the attenuation of the quasi-TE mode of is 0.4 dB/cm at 1.55 μm, while the extinction ratio between the two polarization modes in the waveguide is higher than 25 dB over a region of 80 nm at 1.55 μm. For a waveguide sample with similar length and a smaller ChG thickness (150 nm), the extinction ratio increases to 35 dB. These results demonstrate that the proposed waveguide shows excellent performance as an on-chip polarizer, with high polarization extinction ratio and low insertion loss for the TE mode. Thanks to its simple fabrication process, the proposed waveguide structure provides a convenient way to realize high-quality ChG waveguides, which have great potential in integrated nonlinear optical devices.

Acknowledgment

The authors would like to thank Dr. X. Liu, Electronic Engineering Department, Tsinghua University, for helpful discussions on the simulations of the waveguide bending losses.

References

[1] Y. Yu *et al.*, "A broadband, quasi-continuous, mid-infrared supercontinuum generated in a chalcogenide glass waveguide: Broadband supercontinuum generation in the MIR," *Laser Photon. Rev.*, vol. 8, no. 5, pp. 792–798, Sep. 2014.
[2] T. Wang *et al.*, "Systematic z-scan measurements of the third order nonlinearity of chalcogenide glasses," *Opt. Mater. Exp.*, vol. 4, no. 5, pp. 1011–1022, 2014.
[3] C. Xiong *et al.*, "Generation of correlated photon pairs in a chalcogenide As2S3 waveguide," *Appl. Phys. Lett.*, vol. 98, no. 5, 2011, Art. no. 051101.
[4] J. D. Musgraves *et al.*, "Comparison of the optical, thermal and structural properties of Ge-Sb-S thin films deposited using thermal evaporation and pulsed laser deposition techniques," *Acta Mater.*, vol. 59, no. 12, pp. 5032–5039, Jul. 2011.
[5] R. A. Wibowo, W. S. Kim, E. S. Lee, B. Munir, and K. H. Kim, "Single step preparation of quaternary Cu2ZnSnSe4 thin films by RF magnetron sputtering from binary chalcogenide targets," *J. Phys. Chem. Solids*, vol. 68, no. 10, pp. 1908–1913, Oct. 2007.
[6] A. Abrutis *et al.*, "Hot-wire chemical vapor deposition of chalcogenide materials for phase change memory applications," *Chem. Mater.*, vol. 20, no. 11, pp. 3557–3559, 2008.
[7] S. Levy, M. Klebanov, and A. Zadok, "High-Q ring resonators directly written in As_2S_3 chalcogenide glass films," *Photon. Res.*, vol. 3, no. 3, p. 63, Jun. 2015.
[8] D.-Y. Choi *et al.*, "Thermal annealing of arsenic tri-sulphide thin film and its influence on device performance," *J. Appl. Phys.*, vol. 107, no. 5, 2010, Art. no. 053106.
[9] Y. Zou *et al.*, "Effect of annealing conditions on the physio-chemical properties of spin-coated As_2 Se_3 chalcogenide glass films," *Opt. Mater. Exp.*, vol. 2, no. 12, pp. 1723–1732, 2012.
[10] D.-Y. Choi *et al.*, "Photo-induced and thermal annealing of chalcogenide films for waveguide fabrication," *Phys. Procedia*, vol. 48, pp. 196–205, Jan. 2013.

[11] X. Kong *et al.*, "Fabrication of superconducting magnesium diboride thin films by electron beam annealing," *Supercond. Sci. Technol.*, vol. 24, no. 10, 2011, Art. no. 105013.
[12] J. Eggleton Benjamin, L.-D. Barry, and R. Kathleen, "Chalcogenide photonics," *Nat. Photon.*, vol. 5, no. 12, pp. 141–148, Feb. 2011.
[13] R. Won, "On-chip signal processing," *Nat. Photon.*, vol. 5, no. 12, pp. 725–725, Dec. 2011.
[14] J. Li *et al.*, "Fast crystallization and low-power amorphization of Mg-Sb-Te reversible phase-change films," *CrystEngComm*, vol. 16, no. 32, p. 7401, Jul. 2014.
[15] M. DeJarld *et al.*, "Formation of high aspect ratio GaAs nanostructures with metal-assisted chemical etching," *Nano Lett.*, vol. 11, no. 12, pp. 5259–5263, 2011.
[16] Y. Ruan *et al.*, "Fabrication and characterization of low loss rib chalcogenide waveguides made by dry etching," *Opt. Exp.*, vol. 12, no. 21, pp. 5140–5145, 2004.
[17] J. Hu *et al.*, "Si-CMOS-compatible lift-off fabrication of low-loss planar chalcogenide waveguides," *Opt. Exp.*, vol. 15, no. 19, pp. 11798–11807, Sep. 2007.
[18] X. Gai *et al.*, "Progress in optical waveguides fabricated from chalcogenide glasses," *Opt. Exp.*, vol. 18, no. 25, pp. 26635–26646, 2010.
[19] D.-Y. Choi, S. Maden, A. Rode, R. Wang, and B. Luther-Davies, "Plasma etching of As2S3 films for optical waveguides," *J. Non-Cryst. Solids*, vol. 354, no. 27, pp. 3179–3183, Jun. 2008.
[20] D.-Y. Choi *et al.*, "Submicrometer-thick low-loss As S planar waveguides for nonlinear optical devices," *IEEE Photon. Technol. Lett.*, vol. 22, no. 7, pp. 495–497, Apr. 2010.
[21] T. B. Pittman, B. C. Jacobs, and J. D. Franson, "Heralding single photons from pulsed parametric down-conversion," *Opt. Commun.*, vol. 246, no. 4, pp. 545–550, 2005.
[22] J. Li *et al.*, "Fabrication and characterization of Ge20Sb15Se65 chalcogenide glass rib waveguides for telecommunication wavelengths," *Thin Solid Films*, vol. 545, pp. 462–465, Oct. 2013.
[23] D.-Y. Choi *et al.*, "A protective layer on As2S3 film for photo-resist patterning," *J. Non-Cryst. Solids*, vol. 354, no. 47–51, pp. 5253–5254, 2008.
[24] Y. Zou *et al.*, "Solution processing and resist-free nanoimprint fabrication of thin film chalcogenide glass devices: Inorganic-organic hybrid photonic integration," *Adv. Opt. Mater.*, vol. 2, no. 8, pp. 759–764, Aug. 2014.
[25] Y. Zha, S. Fingerman, S. J. Cantrell, and C. B. Arnold, "Pore formation and removal in solution-processed amorphous arsenic sulfide films," *J. Non-Cryst. Solids*, vol. 369, pp. 11–16, Jun. 2013.
[26] D. Dai, Z. Wang, N. Julian, and J. E. Bowers, "Compact broadband polarizer based on shallowly-etched silicon-on-insulator ridge optical waveguides," *Opt. Exp.*, vol. 18, no. 26, pp. 27404–27415, 2010.
[27] *Refractive Index of As2S3 (Arsenic Trisulfide)—Rodney*, [Accessed: Jan. 27 2016]. [Online]. Available: http://refractiveindex.info/?shelf=main&book=As2S3&page=Rodney.
[28] *Microsoft PowerPoint—SU-8 3000 Data Sheet ver 4.2.ppt—SU-8 3000 Data Sheet.pdf*.
[29] L. Zhang *et al.*, "Silicon waveguide with four zero-dispersion wavelengths and its application in on-chip octave-spanning supercontinuum generation," *Opt. Exp.*, vol. 20, no. 2, pp. 1685–1690, 2012.
[30] Z. Jafari and F. Emami, "Strip/slot hybrid arsenic tri-sulfide waveguide with ultra-flat and low dispersion profile over an ultra-wide bandwidth," *Opt. Lett.*, vol. 38, no. 16, p. 3082, Aug. 2013.
[31] V. Shahraam Afshar and T. M. Monro, "A full vectorial model for pulse propagation in emerging waveguides with subwavelength structures Part I: Kerr nonlinearity," *Opt. Exp.*, vol. 17, no. 4, pp. 2298–2318, 2009.
[32] J. Cheng *et al.*, "Single polarization transmission in pedestal-supported silicon waveguides," *Opt. Lett.*, vol. 36, no. 10, pp. 1797–1799, May 2011.
[33] X. Wu, Y. Sun, J. D. Suter, and X. Fan, "Single mode coupled optofluidic ring resonator dye lasers," *Appl. Phys. Lett.*, vol. 94, no. 24, 2009, Art. no. 241109.
[34] X. Guan *et al.*, "Low-loss ultracompact transverse-magnetic-pass polarizer with a silicon subwavelength grating waveguide," *Opt. Lett.*, vol. 39, no. 15, p. 4514, Aug. 2014.
[35] Q. Wang and S.-T. Ho, "Ultracompact TM-pass silicon nanophotonic waveguide polarizer and design," *IEEE Photon. J.*, vol. 2, no. 1, pp. 49–56, Feb. 2010.
[36] D. Dai and S. He, "A silicon-based hybrid plasmonic waveguide with a metal cap for a nano-scale light confinement," *Opt. Exp.*, vol. 17, no. 19, pp. 16646–16653, Sep. 2009.
[37] L. Sánchez, S. Lechago, and P. Sanchis, "Ultra-compact TE and TM pass polarizers based on vanadium dioxide on silicon," *Opt. Lett.*, vol. 40, no. 7, p. 1452, Apr. 2015.
[38] D. Dai, "Silicon polarization beam splitter based on an asymmetrical evanescent coupling system with three optical waveguides," *J. Light. Technol.*, vol. 30, no. 20, pp. 3281–3287, Oct. 2012.
[39] X. Sun, M. Z. Alam, S. J. Wagner, J. S. Aitchison, and M. Mojahedi, "Experimental demonstration of a hybrid plasmonic transverse electric pass polarizer for a silicon-on-insulator platform," *Opt. Lett.*, vol. 37, no. 23, pp. 4814–4816, 2012.
[40] M. Z. Alam, J. S. Aitchison, and M. Mojahedi, "Compact and silicon-on-insulator-compatible hybrid plasmonic TE-pass polarizer," *Opt. Lett.*, vol. 37, no. 1, pp. 55–57, 2012.
[41] J. N. Caspers, J. S. Aitchison, and M. Mojahedi, "Experimental demonstration of an integrated hybrid plasmonic polarization rotator," *Opt. Lett.*, vol. 38, no. 20, p. 4054, Oct. 2013.
[42] H. Zhang *et al.*, "Efficient and broadband polarization rotator using horizontal slot waveguide for silicon photonics," *Appl. Phys. Lett.*, vol. 101, no. 2, 2012, Art. no. 021105.
[43] L. Li *et al.*, "Integrated flexible chalcogenide glass photonic devices," *Nat. Photon.*, vol. 8, pp. 643–649, 2014.